

# INFLUENCE OF THE CAVITY FIELD FLATNESS AND EFFECT OF THE PHASE REFERENCE LINE ERRORS ON THE BEAM DYNAMICS OF THE ESS LINAC

R. De Prisco\*, Lund University, Lund, Sweden  
R. Zeng, ESS, Lund, Sweden

K. Czuba, T. Leśniak, R. Papis, D. Sikora and M. Żukociński, ISE, Warsaw University of Technology

## Abstract

The particle longitudinal dynamics is affected by errors on the phase and amplitude of the electro-magnetic field in each cavity that cause emittance growth, beam degradation and losses. One of the causes of the phase error is the change of the ambient temperature in the LINAC tunnel, in the stub and in the klystron gallery that induces a phase drift of the signal travelling through the cables and radio frequency components. The field flatness error of each multiple cell cavity is caused by volume perturbation, cell to cell coupling, tuner penetration, etc. In this paper the influences of these two types of errors on the beam dynamics are studied and tolerances for keeping beam quality within acceptable limits are determined.

## INTRODUCTION

The European Spallation Source, ESS, is designed to deliver 5 MW proton beam power on the target while keeping the beam induced losses below 1 W/m throughout the LINAC. This implies the need of accurate models of the accelerating cavities and of the focusing structures to correctly describe the beam dynamics: *only an accurate beam dynamics can allow the calculation of a reliable loss map.*

The use of a simplistic multi-cell cavity model can lead to a wrong estimation of the loss pattern along the accelerator: losses in the normal conducting section, due to a simplistic model, can mask dangerous losses in the high energy part of the LINAC. Vice versa losses in the high energy sections, due to a simplistic model, can lead to an unjustified reductions of the tolerances and, so, to a higher cost. In addition we want to underline that an accurate model of the multi-cell cavities becomes extremely important when one wants to define the tolerances for the sub-systems, as the Low Level RF, LLRF, and the Phase Reference Line, PRL, that induce, usually, errors one order of magnitude smaller than the *static* [1] ones.

In this paper:

- we present a *new* model to calculate the amplitude errors of the accelerating field in a multi-cell cavity: errors are applied on the geometrical parameters of the cavity; then the accelerating field is calculated solving the Maxwell equations over all the cavity;
- we underline the differences between the two models repeating the same error study two times, changing

only the way to calculate the accelerating field within the Drift Tube Linac, DTL, and looking at the beam dynamics parameters at the end of the high- $\beta$  cavities;

- we use the new model to introduce also the flatness errors in the Super Conducting, SC, cavities in order to estimate an acceptable tolerance of their field flatness; these errors were never introduced in all the previous studies;
- we look at the effect of the LLRF phase and amplitude errors and at the Reference Line, RL, phase error errors using the new multi-cell cavity model for all the cavities present in the ESS LINAC.

## THE MULTI-CAVITY MODEL

Let consider a generic cavity of 3 cells, shown in Fig. 1.

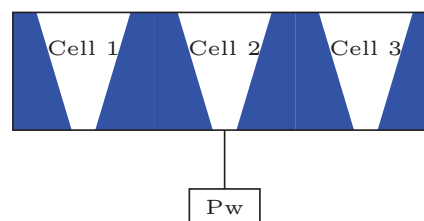


Figure 1: Multi-cell cavity of 3 cells.

It is important to underline that a mechanical error in a cell influences the accelerating field,  $E_0$ , in *all* the cells of the cavity and not only in the cell where the error is located [2].

In the previous error studies [3] [4] the cells of the multi-cell cavities were modeled as a sequence of independent gaps, as shown in Fig. 2, and the errors were applied directly, cell by cell, on the amplitude of the accelerating field, considered a random variable. From now we call this model *old* model.

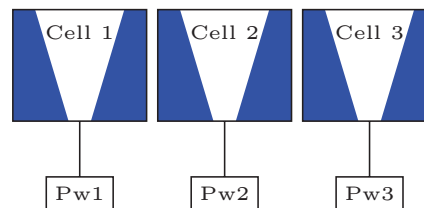


Figure 2: Multi-cell cavity as sequence of independent gaps.

Many particle tracking codes describe all the cells in the same cavity as a sequence of independent one-cell cavities

\* renato.deprisco@ess.se

Content from this work may be used under the terms of the CC BY 3.0 licence (© 2018). Any distribution of this work must maintain attribution to the author(s), title of the work, publisher, and DOI.

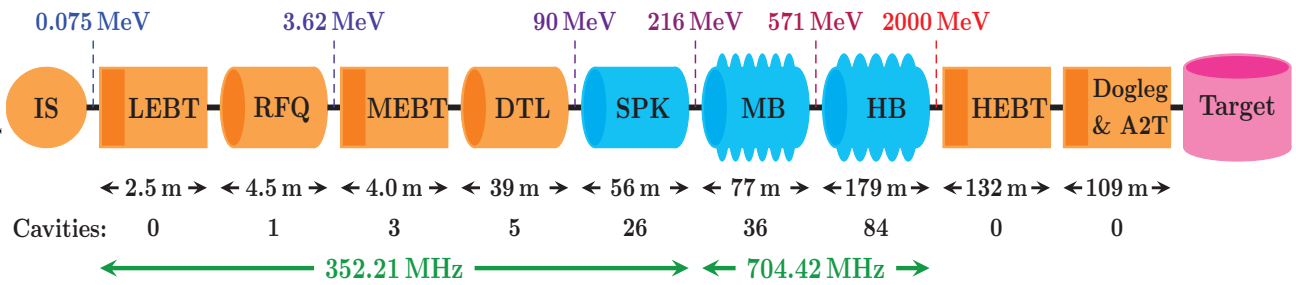


Figure 3: ESS LINAC layout. The beam energy, in MeV, at some locations, is set out above the layout. The length of each section, in m, is set out in the first line below the layout. The number of cavities of each section is set out in the second line below the layout. The operating frequency (green color) of each section is set out in the third line below the layout.

(or gaps). It is up to the user to make sure that the accelerating field of a sequence of independent gaps, that represents a cavity, is a solution of the Maxwell equations within the same cavity.

In this paper, instead, an iterative procedure is defined to calculate  $E_0$  for each cavity: a set of tolerances is specified for all the geometrical parameters of each multi-cell cavity; then the electromagnetic field is calculated solving the Maxwell equations within the same cavity. The algorithm is shown in Fig. 4 where  $E_d$  is the maximum desired accelerating field. From now we call this model *new* model.

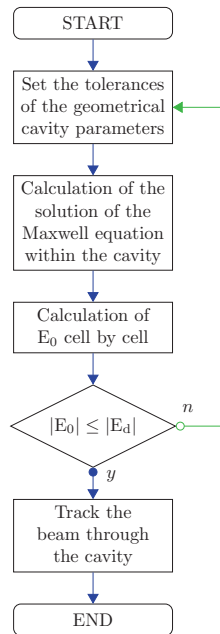


Figure 4: Algorithm to calculate the accelerating field  $E_0$ .

Let consider a SC cavity for example. The geometrical details of a right half cell are shown in Fig. 5: the dome semi-axes are  $A_D$  and  $B_D$ ; the iris semi-axes are  $A_I$  and  $B_I$ ; the full cell length is  $L$ ; the bore radius is  $R_b$ ; the full cavity diameter is  $D$ .

At first the errors are applied individually for each geometrical parameter in order to calculate the *flatness sensitivity*

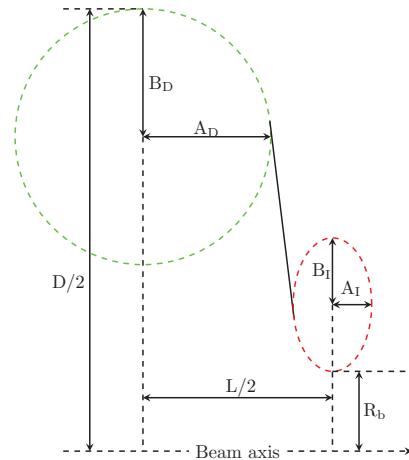


Figure 5: Details of right half cell of SC cavities.

to each parameter. In a second step all the errors are applied simultaneously in order to set the *final* geometrical tolerances that keep the flatness of the accelerating field within the desired limit.

### MULTI-CELL CAVITIES IN THE ESS

The layout of the ESS LINAC [5] [6] is shown in the Fig. 3. The Ion Source, IS, is followed by the Low Energy Beam Transport, LEBT. Then there is the Radio frequency Quadrupole, RFQ, of 4.5 m. Within the Medium Energy Beam Transport, MEBT [7], there are 3 buncher cavities. *These are the only cavities that can be properly simulated using the old model since they are single-cell cavities.* The DTL is composed by 5 multi-cell cavities of 61, 34, 29, 26 and 23 cells [8] [9] and it is followed by 26 Spoke, SPK, cavities. Then there are 36 Medium- $\beta$ , MB [10], cavities of 6 cells each and 84 High- $\beta$ , HB [11], cavities of 5 cells each.

### COMPARISON OF THE TWO MODELS

For the beam dynamics studies reported in this paper the beam is generated at the RFQ input with a gaussian distribution truncated at  $4\sigma$ . The nominal RFQ output distribution is saved and used as input distribution for the rest of the ESS LINAC. The beam parameters at the RFQ output and their

tolerances are reported in the Table 1. The number of particles used is 1 M and the statistic of each study is based on 1000 linacs. The space charge routine used is PICNIC [1].

Table 1: Tolerances of the Beam at the MEBT Input

dx, dy [mm]	dx', dy' [mrad]	dE [keV]	$\Delta\epsilon_{x,y,z}$ [%]	$M_{x,y,z}$ -	dI [mA]
0.3	1	36.2	5	5	0.625

The following *static* [1] errors are included, modeled as random variables uniformly distributed within their tolerances: the quadrupole transverse position, dx, dy, rotation,  $d\phi_x$ ,  $d\phi_y$ ,  $d\phi_z$ , gradient, dG, and multipoles,  $dG_n$  (n=3,4,5), errors; cell field phase,  $d\phi_s$ , error; cavity field,  $dE_k$ , and phase,  $d\phi_k$ , error. The tolerances of the static errors are reported in the Table 2. The subscript B refers to the MEBT, S to the Super Conducting, SC, cavities: spoke, medium- $\beta$  and high- $\beta$  cavities. In red the tolerances related to the flatness of the multi-cell cavities.

Table 2: Static Error Tolerances from the MEBT to HB

Parameter	CAV <sub>B</sub>	DTL	QUAD <sub>B,S</sub>	CAV <sub>S</sub>
dx, dy [mm]	0.5	0.1	0.2	1.5
$d\phi_x, d\phi_y$ [deg]	0.115	0.5	-	0.129
$d\phi_z$ [deg]	-	0.2	0.06	-
$\Delta G$ [%]	-	0.5	0.5	-
$\Delta E_0, \Delta E_k$ [%]	-1	1,1	-, -	5,1
$\Delta\phi_s, \Delta\phi_k$ [deg]	-1	0.5,1	-, -	-,1

The tolerances for the flatness of the accelerating field  $E_0$  in the multi-cell cavities are red-highlighted in the Table 2. The flatness in the DTL is defined as:

$$\Delta E_0 = 100 \cdot \frac{|E_0 - E_d|}{E_d},$$

while for the SC cavities as:

$$\Delta E_0 = 100 \cdot \frac{|E_{p,MAX}| - |E_{p,min}|}{\frac{1}{N} \sum_{c=1}^N |E_{p,c}|},$$

where  $E_{p,c}$  is the peak axial accelerating field in the cell c in a multi-cell cavity of N cells and  $E_{p,MAX}$  and  $E_{p,min}$  the maximum and the minimum peak respectively.

To compare the two models we perform two error studies (up to the high- $\beta$  cavities) where the errors are changed in the same way linac by linac. The only difference is the method used to calculate the accelerating field into the DTL [8] [12] [13]: in the first study we use the new model, in the second one the error of the accelerating field  $E_0$ , cell by cell, is modeled as a random variable uniformly distributed within its tolerance. The field flatness is kept within 1% in the DTL [14] on top of the *nominal*  $E_0$  [15] and within 5% in the SC cavities. It is important to underline that, from this moment, we suppose that the interfaces of the DTL and the DTL stabilization system are *fully integrated* [16] in the

design to avoid the *self perturbation phenomena* [15] of these components. We remember, again, that to compare the two models only the *static* [1] errors are considered.

The RMS emittance growths in the horizontal,  $\Delta\epsilon_x$ , vertical,  $\Delta\epsilon_y$ , and longitudinal,  $\Delta\epsilon_z$ , plane at the end of the high- $\beta$  cavities are shown in Fig. 6. It is evident that the old model underestimates hugely the emittance growths in all the planes.

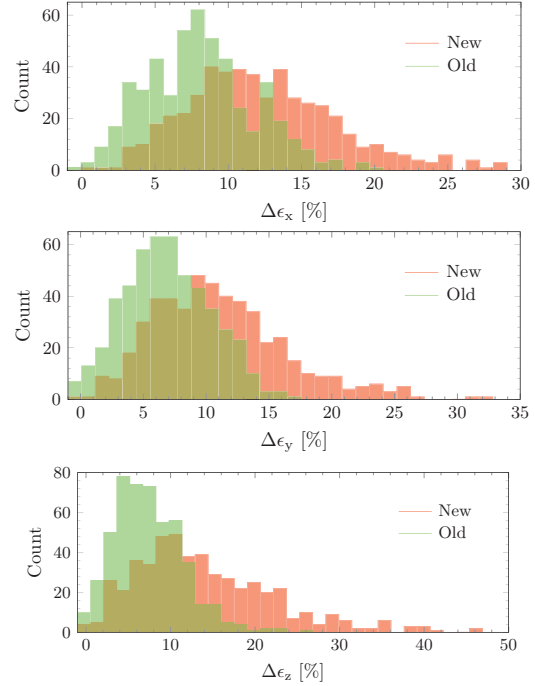


Figure 6: From top to bottom: Additional RMS emittance growth in the horizontal,  $\Delta\epsilon_x$ , vertical,  $\Delta\epsilon_y$ , and longitudinal,  $\Delta\epsilon_z$ , plane at the end of the high- $\beta$  cavities. The red color indicates that the accelerating field into the DTL is calculated solving the Maxwell equations (new method) while the green color indicates that  $E_0$ , within the DTL, is modeled as a random variable uniformly distributed within its tolerance (1%).

To emphasize the difference of the two models in the Fig. 7 is shown the longitudinal halo parameter  $h_z$ .

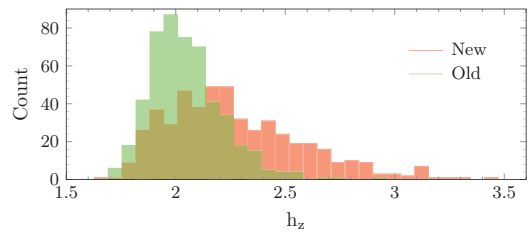


Figure 7: Halo Parameter,  $h_z$ , at the end of the high- $\beta$  cavities when the flatness of  $E_0$ , within the DTL, is 1%. The difference in the histograms is due *only* to the modelization of the accelerating field into the DTL since all the other errors are the same linac by linac.

Content from this work may be used under the terms of the CC BY 3.0 licence (© 2018). Any distribution of this work must maintain attribution to the author(s), title of the work, publisher, and DOI.

The comparison clearly shows that the new cavity model is very important to model the long multi-cell cavities as the DTL: the tolerance of the flatness in the long multi-cell cavities has a huge impact on the beam parameters of the downstream sections. The emittance growth and the halo on the longitudinal plane increase the probability to have particles which are not captured by the RF bucket after the frequency transition (352,21MHz/704,42MHz) at the interface SPOKE/MEDIUM- $\beta$  cavities.

## PHASE REFERENCE LINE

The Phase Reference Distribution System, PRDS, shown in Fig. 8, consists of two sub-systems: the main PRDS, called PRL, and the local PRDS (from the PRL outputs, in the tunnel, to the devices in the klystron gallery). The main PRDS is an in-kind contribution from ISE, Warsaw University of Technology [17] [18]. The main PRDS can be divided in the PRL, the PRL temperature control system, the PRL pressure and humidity control system and the PRL data acquisition and monitoring system. The PRDS design is based on 3 fundamental assumptions:

1. the first assumption is to use a passive synchronization scheme where the pick-up cables from RF cavities and BPMs/LBMs are paired and length-matched to the corresponding reference cables from the PRDS. This minimizes the phase drift errors between these 2 cables and enables precise synchronization since both cables are exposed to the same environment conditions and experience the same drift. This allows to make the main PRDS totally passive and to place it in the accelerator tunnel where other synchronization systems with active drift compensation techniques cannot be used;
2. the second assumption is to distribute two phase reference sinusoidal signals: 352.21 MHz and 704.42 MHz since there are accelerating cavities operating at both frequencies;
3. the third fundamental assumption is to use the same physical structure to distribute both frequencies because of the limited space in the accelerator tunnel.

The two phase reference sine waves, at 352 MHz and at 704 MHz, are synthesized in the Master Oscillator, MO, source and, then, amplified to the level of  $\sim +50$  dBm each in the high power amplifier stage. This is done in MO racks located in the klystron gallery. The two-tone high-power signal is, then, transmitted with a single 7/8" flexible cable from the gallery down to the tunnel through a stub. Here the signal is split by a high power divider and is sent to the two branches of the main line.

The PRL is the backbone of the ESS accelerator synchronization system. It provides the phase reference signals for LLRF systems, BPM, Beam Position Monitor, systems and LBM, Longitudinal Beam Monitor, systems with low phase noise and low phase drifts all along the  $\sim 600$  m long machine. There are 155 LLRF systems, 101 BPM systems and

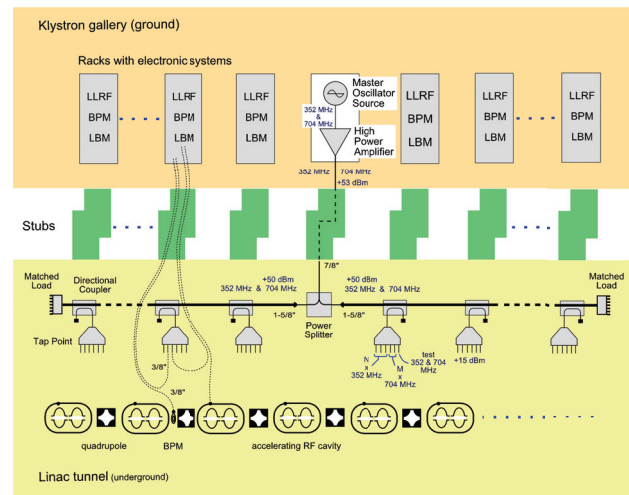


Figure 8: Conceptual schematic of the PRDS.

4 LBM. The PRL itself is  $\sim 581$  m long according to the current design. It starts at  $\sim 7$  m from the IS and ends  $\sim 15$  m before the target. It means that the PRL is located along the entire length of the tunnel ( $\sim 540$  m) and enters in the target building.

The line is suspended from the ceiling and it is above the accelerator components. The input of the main line is located in the  $\sim$ middle of the line itself. There are two branches: one toward the ion source and another one toward the target. This solution minimizes the power drop due to the attenuation in the transmission line. The two branches are terminated with matched loads to minimize the reflections. The line is an air-filled coaxial transmission type. It is realized in 1-5/8" rigid coax standard due to relatively low attenuation and temperature drifts.

The main line provides the reference signal to 58 Tap Points, TPs, located in different positions along the tunnel: custom designed directional couplers transmit a portion of the reference signal from the main line to the TPs. The couplers are located in the TP positions. The TPs are custom designed modules which split the input reference signal into multiple outputs. In this way just one TP, associated to a coupler, provides multiple signals to many instruments which are in close proximity in the tunnel. This solution allow to save space and to reduce costs: dedicated couplers for each reference output without multi-channel TPs would be significantly more expensive and impractical for the ESS.

Each TP becomes crucial for the temperature stabilization because of the significant heat transfer related to the cables connected to the PRL in the TP positions. This is why each TP has a dedicated temperature control loop which has to ensure temperature stable boarder conditions to the temperature control system.

A cavity pick-up signal cable is bundled together with the corresponding reference cable from the TP and this length-matched cable pair goes to LLRF rack. Similarly, a probe signal cable from each BPM/LBM is bundled together with the corresponding reference cable from the tap point and this

length-matched cable pair goes to BPM/LBM rack. This solution minimizes the phase drift errors between the two cables in the pair and enables precise synchronization since both cables are exposed to the same environment conditions and experience the same drifts.

The point where the phase stabilization begins is the input to the high power amplifiers shown in Fig. 8. This point represents the phase reference fiducial in the signal distribution system from where the phase errors are controlled and minimized. In the tunnel the signal phase is stabilized, indirectly, controlling the environment conditions (temperature, pressure, humidity) while in the the MO racks and *from the MO to the tunnel the signal phase is stabilized, directly, using active electronic signal phase compensation.*

Since the physical length of a coaxial cable changes as the temperature of the cable changes, inducing a signal phase drift, the temperature around the cable has to be controlled within a small variation to reduce phase drift. Basing on measurements, the phase drift of a 1-5/8" rigid line is  $\sim 8.48^\circ/\text{C}$  over 600 meters (the temperature coefficient is  $\sim 0.0141^\circ/\text{C}/\text{m}$ ). Therefore the temperature of the cable should be kept within  $\pm 0.1^\circ\text{C}$  to maintain the phase stability within  $\pm 1^\circ$  over the whole LINAC. The easiest way to meet this requirement is to heat up the rigid line to few degrees above ambient temperature using a heating cable wrapped around the outer conductor and to stabilize it using a feedback loop. A thermal insulation will be placed on the coaxial rigid line to equalize the temperature along the line and to slow down its cooling. The thickness of the insulation should not exceed 40 mm basing on simulations and measurements made at the Lund University.

The pressure and humidity control system is responsible for control and stabilization of pressure and humidity in the PRL. Humidity stabilization is achieved by filling the PRL with nitrogen gas which is dry thus solves problem of atmospheric air humidity changes. Pressure stabilization is realized with pneumatic automation system that controls pressure of the nitrogen gas in the PRL.

## GLOBAL ERROR STUDY

A final end to end error study is performed to analyze the effect of all the errors together including the LLRF errors and the PRL phase errors. The LLRF errors are modeled as gaussian random variables with zero-average and standard deviation set out in the Table 3.

Table 3: Dynamic [1] Errors Tolerances

Parameter	CAV <sub>B</sub>	DTL	CAV <sub>S</sub>
$\Delta E_k$ [%]	0.2	0.2	0.1
$\Delta \phi_k$ [deg]	0.2	0.2	0.1

The PRL phase errors are modeled so that:

- the phase difference between two consecutive cavities does not exceed  $0.05^\circ$ ;

- the phase difference between two generic points in the ESS LINAC does not exceed  $2^\circ$ .

The static errors applied after the high- $\beta$  cavities are set out in Table 4.

Table 4: Static Error Tolerances After the High- $\beta$  Cavities

Parameter	QUAD	DIP
$dx, dy$ [mm]	0.2	0.2
$d\phi_x, d\phi_y$ [deg]	0	0
$d\phi_z$ [deg]	0.06	0.06
$\Delta G$ [%]	0.5	0.05

The power losses, shown in Fig. 9, are due, mainly, to the particles which were in the tail of the beam at the RFQ output or which have not been captured inside the RF bucket after the frequency transition (352,21MHz/704,42MHz) at the interface SPOKE/MEDIUM- $\beta$  cavities.

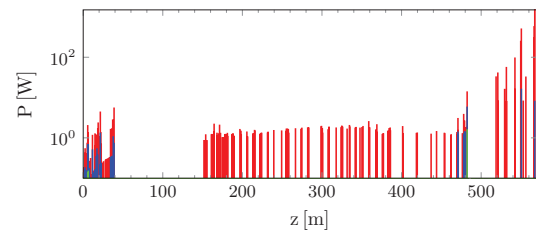


Figure 9: Power loss (per element) at 100% (red), 99% (blue) and 95% (green) confidence levels along the ESS LINAC.

## CONCLUSION

The cavity model is important for the reliability of the beam dynamics parameters and of the power loss map: losses in the normal conducting section, due to a simplistic model, can mask dangerous losses in the high energy part of the LINAC. Vice versa losses in the SC section, due to a simplistic model, can lead to an unjustified reductions of the tolerances and, so, to a higher cost.

The studies show that modeling the error of the accelerating field, cell by cell in a multi-cell cavity, as a random variable, uniformly distributed within its tolerance, causes an underestimation of the emittance growth and of the halo parameters. The larger the number of cells is in a multi-cell cavity, the higher the underestimation of the beam dynamics parameters is. This means that the new cavity model is very important for the long multi-cell cavities as the DTL.

In the case of the ESS LINAC the global error study with the new model of the multi-cell cavities shows that the considered tolerances, including the SC flatness errors and RL phase errors, give a loss map more dense than the maps of the previous studies in the worst cases, but the loss peaks are compatible with the power level considered acceptable in the previous studies.

The beam in this study is generated at the RFQ entrance: a realist beam out of the IS may cause more losses.

## REFERENCES

- [1] R. De Prisco *et al.*, “ERROR study on normal conducting ESS LINAC,” in *Proc. 27th Linear Accelerator Conf. (LINAC’14)*, Geneva, Switzerland, September 2014, paper THPP042, pp. 942–944.
- [2] R. De Prisco *et al.*, “ESS DTL RF modelization: field tuning and stabilization,” in *Proc. 4th Int. Particle Accelerator Conf. (IPAC’13)*, Shanghai, China, May 2013, paper THPWO070, pp. 3918–3920.
- [3] M. Eshraqi *et al.*, “Statistical error studies in the ESS LINAC,” in *Proc. 5th Int. Particle Accelerator Conf. (IPAC’14)*, Dresden, Germany, June 2014, paper THPME044, pp. 3323–3325.
- [4] Y. Levinsen *et al.*, “Beam dynamics challenges in the ESS LINAC,” in *Proc. 57th ICFA Advanced Beam Dynamics Workshop on High-Intensity and High-Brightness Hadron Beams (HB’16)*, Malmö, Sweden, July 2016, paper THPME044, pp. 315–318.
- [5] M. Lindroos *et al.*, “ESS Progressing into Construction,” in *Proc. 7th Int. Particle Accelerator Conf. (IPAC’16)*, Busan, Korea, May 2016, paper FRYAA02, pp. 4266–4270.
- [6] A. Ponton *et al.*, “ESS Normal Conducting Linac Status and Plans,” in *Proc. 27th Linear Accelerator Conf. (LINAC’14)*, Geneva, Switzerland, September 2014, paper THPP044, pp. 948–950.
- [7] R. Miyamoto *et al.*, “Beam Physics Design of the ESS Medium Energy Beam Transport,” in *Proc. 5th Int. Particle Accelerator Conf. (IPAC’14)*, Dresden, Germany, June 2014, paper THPME045, pp. 3326–3328.
- [8] R. De Prisco *et al.*, “ESS DTL status: redesign and optimizations,” in *Proc. 5th Int. Particle Accelerator Conf. (IPAC’14)*, Dresden, Germany, June 2014, paper TUAM3Y01, pp. 3314–3316.
- [9] M. Comunian, F. Grespan, and A. Pisent, “ERROR study on normal conducting ESS LINAC,” in *Proc. 27th Linear Accelerator Conf. (LINAC’14)*, Geneva, Switzerland, September 2014, paper THPP086, pp. 1047–1049.
- [10] P. Michelato *et al.*, “INFN Milano - LASA activities for ESS,” in *Proc. 17th Int. Conf. on RF Superconductivity (SRF’15)*, Whistler, Canada, September 2015, paper FRIOC02, pp. 1081–1084.
- [11] G. Devanz *et al.*, “ESS elliptical cavities and cryomodules,” in *Proc. 16th Int. Conf. on RF Superconductivity (SRF’13)*, Paris, France, September 2013, paper FRIOC02, pp. 1218–1222.
- [12] F. Grespan *et al.*, “ESS DTL Design and Drift Tube Prototypes,” in *Proc. 27th Linear Accelerator Conf. (LINAC’14)*, Geneva, Switzerland, September 2014, paper THPP044, pp. 1050–1052.
- [13] F. Grespan, “RF properties of the tank 5, pickup, RF coupler, RF windows, post coupler, thermo-mechanical simulations, field tuning, tuning in operation,” <http://indico.esss.lu.se/event/348/session/3/material/2/0.pptx>
- [14] R. De Prisco *et al.*, “Implication of manufacturing errors on the layout of the stabilization system and on the field quality in a drift tube linac - RF DTL error study,” in *Proc. 28th Linear Accelerator Conf. (LINAC’16)*, East Lansing, Michigan, September 2016, paper MOPLR68, pp. 290–293.
- [15] R. De Prisco *et al.*, “Effect of the field maps on the beam dynamics of the ESS drift tube LINAC,” in *Proc. 6th Int. Particle Accelerator Conf. (IPAC’15)*, Richmond, Virginia, May 2015, paper THPF078, pp. 3864–3866.
- [16] R. De Prisco *et al.*, “Integration of interfaces and stabilization system in the design of a drift tube linac,” in *Proc. 28th Linear Accelerator Conf. (LINAC’16)*, East Lansing, Michigan, September 2016, paper MOPLR70, pp. 294–297.
- [17] M. Żukocinski *et al.*, “Phase reference distribution system for European Spallation Source,” <http://www.l1rf2017.org/pdf/Posters/P-95.pdf>
- [18] K. Czuba *et al.*, “Concept of the phase reference line for the European Spallation Source,” in *Proc. 22th Int. Microwave and Radar Conf. (MIKON’18)*, Poznań, Poland, May 2018.